nature materials

ARTICLES

PUBLISHED ONLINE: 5 OCTOBER 2015 | DOI: 10.1038/NMAT4428

Understanding and predicting the orientation of heteroleptic phosphors in organic light-emitting materials

Matthew J. Jurow[1], Christian Mayr[2], Tobias D. Schmidt[2], Thomas Lampe[2], Peter I. Djurovich[1], Wolfgang Brütting[2] and Mark E. Thompson[1]*

Controlling the alignment of the emitting molecules used as dopants in organic light-emitting diodes is an effective strategy to improve the outcoupling efficiency of these devices. To explore the mechanism behind the orientation of dopants in films of organic host materials, we synthesized a coumarin-based ligand that was cyclometalated onto an iridium core to form three phosphorescent heteroleptic molecules, $(bppo)_2Ir(acac)$, $(bppo)_2Ir(ppy)$ and $(ppy)_2Ir(bppo)$ (bppo represents benzopyranopyridinone, ppy represents 2-phenylpyridinate, and acac represents acetylacetonate). Each emitter was doped into a 4,4′-bis(*N*-carbazolyl)-1,1′-biphenyl host layer, and the resultant orientation of their transition dipole moment vectors was measured by angle-dependent *p*-polarized photoluminescent emission spectroscopy. In solid films, $(bppo)_2Ir(acac)$ is found to have a largely horizontal transition dipole vector orientation relative to the substrate, whereas $(ppy)_2Ir(bppo)$ and $(bppo)_2Ir(ppy)$ are isotropic. We propose that the inherent asymmetry at the surface of the growing film promotes dopant alignment in these otherwise amorphous films. Modelling the net orientation of the transition dipole moments of these materials yields general design rules for further improving horizontal orientation.

Molecular orientation and solid-state morphology exert a significant impact on the performance of molecular electronic devices[1–5]. The use of phosphorescent iridium complexes with near-unity electroluminescence quantum yields as emitters in modern organic light-emitting diodes (OLEDs) has allowed for the manufacture of devices with excellent efficiencies[6,7]. Despite high internal quantum efficiencies, approximately 80% of photons are trapped inside the thin-film structure and lost to surface plasmons and waveguide modes. To reduce the incidence of photons being dissipated to these loss channels, and enhance external quantum efficiencies (EQEs), outcoupling technologies have been successfully employed[8–10]. An alternative strategy to address this problem is to intrinsically increase the outcoupling efficiency through control of the direction of light emission. The organometallic molecules at the core of these devices emit light perpendicular to their transition dipole moment vector[4,11] (TDV). Orienting emissive molecules with transition dipoles parallel to the substrate would eliminate the need for micro-lens arrays, gratings or other physical methods used to enhance outcoupling, and allow for large-scale manufacture of OLEDs with high EQEs (refs 4,8,9,12–14).

Isotropic dopant orientation is observed in films of facial tris-iridium phenylpyridine ($Ir(ppy)_3$) and many other homoleptic tris-cyclometalated Ir dopants[15–17]. Heteroleptic complexes of the formula $(C^{\wedge}N)_2Ir(O^{\wedge}O)$, where $C^{\wedge}N$ is a cyclometalated ligand and $O^{\wedge}O$ is a diketonate ligand such as acetylacetonate (acac), have previously been observed to demonstrate higher EQEs than their homoleptic $Ir(C^{\wedge}N)_3$ analogues, because their average TDVs are disproportionately horizontal relative to the substrate in solid films[11,16–25]. There are numerous reports of other dopants with ancillary ligands, especially acac and its close analogues, which feature net parallel TDV orientations to various degrees in doped films (see Supplementary Table 1 for tabulated literature data)[22–25].

Two mechanisms have been invoked to account for the disparity in the alignment properties of selected dopants in an otherwise amorphous or nearly amorphous host matrix. Past reports have speculated that large dipole moments present in the tris-cyclometalates lead to aggregation that suppresses dopant interactions with the host matrix[16,26–28]. Other reports have proposed electrostatic interactions between electronegative regions in the $(C^{\wedge}N)_2Ir(O^{\wedge}O)$ complexes and electropositive host structures give rise to macroscopic order and thus dopant (and host) alignment[22,29,30]. We will show that neither the dopant dipole-based mechanism nor component electrostatics adequately describe the alignment process and propose a mechanism based on the inherent asymmetry of $(C^{\wedge}N)_2Ir(O^{\wedge}O)$ and some fac-$Ir(C^{\wedge}N)_3$ complexes that explain the many instances of observed dopant alignment in amorphous host materials.

To explore the mechanism by which these approximately spherical phosphors orient in amorphous host materials we synthesized a coumarin-based ligand from which we prepared heteroleptic iridium-based emitters: $(bppo)_2Ir(acac)$, $(bppo)_2Ir(ppy)$ and $(ppy)_2Ir(bppo)$, where bppo represents benzopyranopyridinone, and ppy represents 2-phenylpyridinate (Fig. 1). The coumarin functionality was employed because the carbonyl (C=O) group provides a large dipole moment[15,17]. Each material was doped into a 4,4′-bis(*N*-carbazolyl)-1,1′-biphenyl (CBP) host matrix at 2, 6, 12 and 20% (v/v) and characterized by angle-dependent *p*-polarized emission (see Methods for details). Analysis of emission from films containing $(bppo)_2Ir(acac)$ reveals that dopant TDVs are oriented

[1]Department of Chemistry, University of Southern California, Los Angeles, California 90089, USA. [2]Institute of Physics, University of Augsburg, 86135 Augsburg, Germany. *e-mail: met@usc.edu

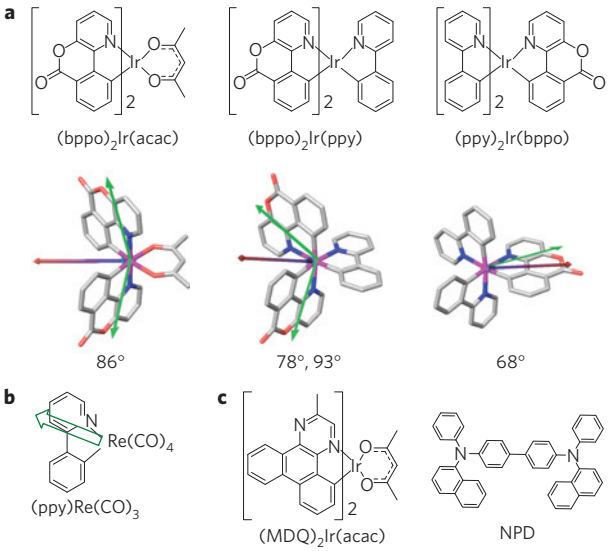

Figure 1 | Material structure and properties. a, Structures of phosphorescent dopants used here. Listed below each structure are the angle(s) between the permanent (μ, red arrows) and transition dipole vectors (TDVs, green arrows). The dipole moment of $(bppo)_2Ir(acac)$ ($\mu = 6.18$ D) lies along the molecular C_2 axis. In $(bppo)_2Ir(ppy)$ the dipole ($\mu = 8.44$ D) is tilted from this axis and lies in a plane of the bppo ligand that is trans to the C_{bppo} and N_{ppy}. In $Ir(ppy)_2(bbpo)$ the dipole ($\mu = 8.25$ D) lies in the plane of the ppy ligand that is also *trans* to C_{bppo} and N_{ppy} but is tilted towards the bppo ligand. **b**, TDV orientation measured in $(ppy)Re(CO)_4$ (TDV, green arrow). **c**, Structures of $(MDQ)_2Ir(acac)$ and NPD.

with a net horizontal alignment, whereas the emission from films with $(ppy)_2Ir(bppo)$ and $(bppo)_2Ir(ppy)$ is indicative of nearly isotropic orientation, although the dopants have substantial permanent dipole moments and similarly oriented TDVs. Understanding the causes of the alignment behaviour will allow us to develop dopant molecules that will preferentially orient in films of isotropic materials for diverse uses in photonic devices.

Results

The synthesis and photophysical properties of $(bppo)_2Ir(ppy)$ and $(ppy)_2Ir(bppo)$ have been reported previously[31]. A reaction between $[Ir(bppo)_2(\mu\text{-}Cl)]_2$ and ppy-H formed both $(bppo)_2Ir(ppy)$ and $(ppy)_2Ir(bppo)$ in moderate yield. Both complexes were isolated as facial isomers, with the $(ppy)_2Ir(bppo)$ species being a result of ligand scrambling during the course of the reaction. See Methods for synthetic details and synthesis of $(bppo)_2Ir(acac)$. The Ir complexes exhibit photophysical properties typical of phosphorescent iridium complexes. At room temperature the compounds exhibit strong green–yellow luminescence, and have quantum yields of greater than 88% and luminescence decay times in the microsecond range in solution (see Supplementary Information). Ground-state dipole moments for the complexes were calculated using density functional theory[32–35] (B3LYP-LACVP**; Fig. 1).

Films of the complexes doped into CBP were vapour deposited at 2, 6, 12 and 20% (v/v) to probe the impact of dipole moment and heteroleptic substitution on aggregation and concentration quenching. All species have large quantum yields in solid films, greater than 30% at any doping level tested. Concentration-related quenching of photoluminescent quantum yield, along with a bathochromic shift of emission indicative of dopant aggregation in the solid films, was observed with all species. The extent of the concentration quenching varied between the three dopants, with the $(bppo)_2Ir(ppy)$ species showing the largest loss in quantum yield, followed by $(bppo)_2Ir(acac)$ and finally $(ppy)_2Ir(bppo)$. As concentration quenching requires an overlap of the emissive ligands, we believe that the $(bppo)_2Ir(ppy)$ demonstrates the largest effect because it has two potentially emissive ligands.

Angle-dependent *p*-polarized emission measurements of doped films by photoluminescent excitation are used to determine the net orientation of the TDVs of emissive dopants[4,12,23,25,36–38]. We define the value Θ as the ratio of power radiated by vertical components of the contributing TDVs to the total power radiation. The details of this measurement are given in the Methods. A film with isotropic phosphors will yield a value of $\Theta = 0.33$. If the emissive TDV is aligned parallel to the substrate, $\Theta = 0$. A film with the TDV perpendicular to the substrate will give $\Theta = 1$. Vertically oriented transition dipoles couple strongly to surface plasmons in the metal electrodes of the OLED, decreasing the external efficiency of the OLED; therefore, the smallest possible value of Θ is desired[36,39].

Emission from $(ppy)_2Ir(bppo)$ and $(bppo)_2Ir(ppy)$ was observed to be nearly isotropic at all measured doping levels. Films doped with $(bppo)_2Ir(acac)$ exhibit $\Theta = 0.22$ (Fig. 2), similar to the value observed for other heteroleptic iridium complexes with β-diketonate ligands. Interestingly, we observed that films doped with $(bppo)_2Ir(acac)$ exhibit $\Theta = 0.22$ independent of doping concentration between 6 and 20% with nearly identical line fits, despite being well into the concentration quenched regime (indicative of significant aggregation).

Discussion

Previous studies have reported that the magnitude of the ground-state dipole moment of the emitter effects the degree of aggregation and thus alignment and emission characteristics of iridium complexes in doped films[26]. Aggregated complexes were proposed to undergo a decreased interaction with the host matrix and randomly orient[40]. All tested dopants here exhibit spectral broadening and concentration quenching due to aggregation (see Supplementary Information) as expected because of their large permanent dipole moments. The concurrent observed redshifted emission in doped films indicates that these aggregates emit photons. The unchanged orientation measured in the extremely concentrated (20% v/v) $(bppo)_2Ir(acac)$ film implies that the lack of aggregation is not responsible for the consistently observed net horizontal TDV orientation of heteroleptic iridium complexes containing an acac ligand.

To understand the observed alignment for the bppo and related $Ir(C\hat{}N)_3$ and heteroleptic complexes, it is essential to be able to define the orientation of the TDV relative to the molecular frame, because our optical measurement gives only the relationship of the TDV to the substrate plane. Emission from cyclometalated iridium complexes is due predominantly to a triplet metal-to-ligand-charge-transfer (^{3}MLCT) transition. In a heteroleptic Ir complex, emission is expected to originate from a ^{3}MLCT state involving the ligand(s) with the lowest triplet energy[41]. Calculated triplet spin density surfaces indicate that all three bppo-based complexes considered here emit from a ^{3}MLCT state involving a single bppo ligand. The next step is to determine the orientation of the TDV for the '(bppo)Ir' fragment and ultimately to the permanent dipole moment of the molecule. Fortunately, the orientation of the TDV has been determined experimentally for the closely related cyclometalated complex $(ppy)Re(CO)_4$ by examining the polarization of emission obtained from a single crystal[42]. This Re complex emits from a ^{3}MLCT involving the '(ppy)Re' fragment. The TDV was found to lie in the plane of the ppy ligand directed by an angle of $\delta = 18.5°$ away from the Re–N bond axis (Fig. 1b). Considering that the molecular and photophysical properties of $(bppo)_2Ir(acac)$ are similar to those of $(ppy)_2Ir(acac)$, the orientation of the transition dipole for the two cyclometalated ligands can be expected to lie in a similar direction. The electron-withdrawing nature of the carbonyl functionality of the bppo ligand is expected to shift the TDV further away from the

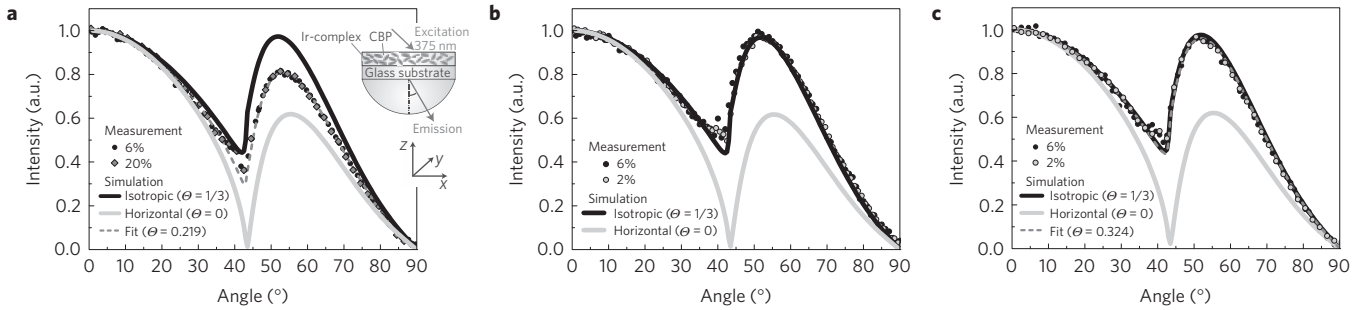

Figure 2 | Polarized emission spectra. a–c, Cross-sections of the measurements and simulations of the angle-dependent *p*-polarized photoluminescence emission spectra (considering an emission in the *x*–*z* plane) for films of 15 nm CBP doped with $(bppo)_2Ir(acac)$ (at 540 nm) (**a**), $(bppo)_2Ir(ppy)$ (at 530 nm) (**b**) and $(ppy)_2Ir(bppo)$ (at 550 nm) (**c**) at different doping levels on glass substrates. The measured data have been fitted (dashed lines) to determine the degree of orientation. $(bppo)_2Ir(acac)$ $\Theta = 0.22$; $(bppo)_2Ir(ppy)$ $\Theta = 0.33$; and $(ppy)_2Ir(bppo)$ $\Theta = 0.32$. Inset image in **a** depicts experimental design.

Ir–N bond than is observed for $(ppy)Re(CO)_4$; thus, we expect the bppo-based emitters to give an angle between the Ir–N bond and the TDV, defined as δ, between 20° and 40°.

The angles between the permanent and transition dipole moments for each bppo-based dopant are illustrated in Fig. 1a, assuming a δ value of 20°. With two identical emissive bppo ligands, $(bppo)_2Ir(acac)$ and $(bppo)_2Ir(ppy)$ have similar angles between their ground-state and transition dipole moment vectors, averaging 86°. $(ppy)_2Ir(bppo)$ has a slightly smaller angle of 68°. The similarities of these angles, contrasted with the observation that only $(bppo)_2Ir(acac)$ shows a net alignment in doped films, further indicates that the permanent molecular dipole is not responsible for dopant alignment in Ir-phosphor-based films.

Previous reports have suggested that simultaneous host and dopant interactions in aligned matrices arise from the formation of donor/host aggregates based on the component electrostatics[22,29,30]. The complexes studied here have very similar electrostatic surfaces (Fig. 3). $(bppo)_2Ir(acac)$ and $(bppo)_2Ir(ppy)$ are both dominated by the strongly electronegative coumarin ligand, yet demonstrate quite different orientation behaviour in CBP. Thus, component electrostatics is unlikely to be an important factor in alignment for these dopants.

A mechanism for molecular alignment of a growing thin film of neat organic molecules during vacuum deposition has been described previously[43,44]. These authors propose that molecules with high aspect ratios, such as CBP or NPD, preferentially lie with their long axis parallel to the surface, thus minimizing the surface free energy and increasing the film density. The CBP host used here has a comparatively low glass transition temperature ($T_g = 62$ °C; ref. 45), which the previous report predicts should give an isotopic film. A separate recent study has found no dependence of the TDV orientation of two prototypical heteroleptic emitters ($(ppy)_2Ir(acac)$ and $(MDQ)_2Ir(acac)$) on the T_g of the host material, with observed dopant ordering resulting from intrinsic properties of the dopant species[17].

Here we propose a mechanism, extending from previous reports on neat films[43,44], that recognizes a surface of an amorphous (isotropic) film as inherently asymmetric during deposition, that is, organic film versus vacuum, which leads to the alignment of molecules deposited on it. The acac group presents an aliphatic region on the surface of the $(C^{\wedge}N)_2Ir(acac)$ complex, which lies along the molecular C_2 axis. We propose that the boundary created between the organic host material on the substrate and the vacuum of the deposition chamber during fabrication causes the asymmetrical $(C^{\wedge}N)_2Ir(acac)$ molecules to orient before it is over coated with an amorphous layer of the host material. Molecular rearrangement and alignment on surfaces is known to occur on timescales consistent with this mechanism[43,46–48]. Note that this mechanism does not require any alignment of the host material, and explains why $(C^{\wedge}N)_2Ir(O^{\wedge}O)$ phosphors with widely varied cyclometallating ligands all show similar degrees of dopant alignment (see Supplementary Information for tabulated values), because the shared β-diketonate ligand will give a discrete aliphatic surface 'patch' in each case.

Support for a surface-promoted alignment of dopants is seen in the recent report of an isotropic orientation for $(ppy)_2Ir(acac)$ when spin-cast in a poly-methylmethacrylate matrix (the same dopant gives $\Theta = 0.22$ in vapour deposited films)[30]. We have also examined solution-deposited films of $Ir(ppy)_3$, $(MDQ)_2Ir(acac)$ and $(bppo)_2Ir(acac)$ doped in poly-methylmethacrylate and observed emission indicative of isotropic orientation. Previous reports have shown a similar difference when comparing solution processed and thermally evaporated organic thin films, that is, isotropic and ordered films, respectively, from the two methods[44,49]. The isotropic nature of the films processed from solution supports our proposal that an organic/vacuum interface is needed for dopant alignment. It is important to note that the vacuum and solution deposited films are in different host materials. Unfortunately, the poor solubility of CBP prevents direct comparison between vacuum and solution processing. To further test our hypothesis we compared films prepared by both vacuum deposition and spin-coating a solution of $(MDQ)_2Ir(acac)$ doped into NPD (8% v/v; see Fig. 1). The spin-cast films exhibited an orientation of $\Theta = 0.36$, that is, nearly isotropic (see Supplementary Information). When fabricated by vapour deposition, the same system demonstrates horizontal orientation with $\Theta = 0.24$, in good agreement with the reported values of alignment for $(C^{\wedge}N)_2Ir(acac)$ dopants[26]. This result indicates that the vacuum/organic boundary created during vapour deposition is critical to producing the observed alignment in the measured heteroleptic systems.

To assess consequences of dopant alignment we have developed a mathematical representation that illustrates how the orientation

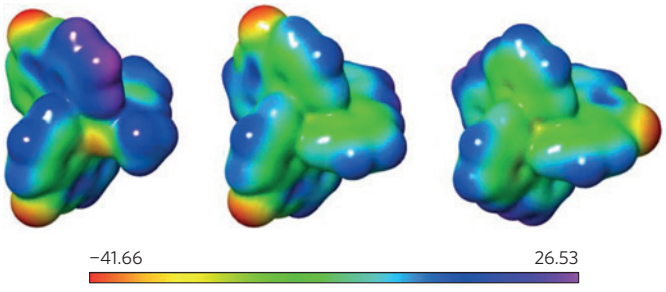

Figure 3 | Electrostatic surfaces. Calculated electrostatic surface potentials (kcal mol^{-1}) for $(bppo)_2Ir(acac)$ (left), $(bppo)_2Ir(ppy)$ (middle) and $(ppy)_2Ir(bppo)$ (right).

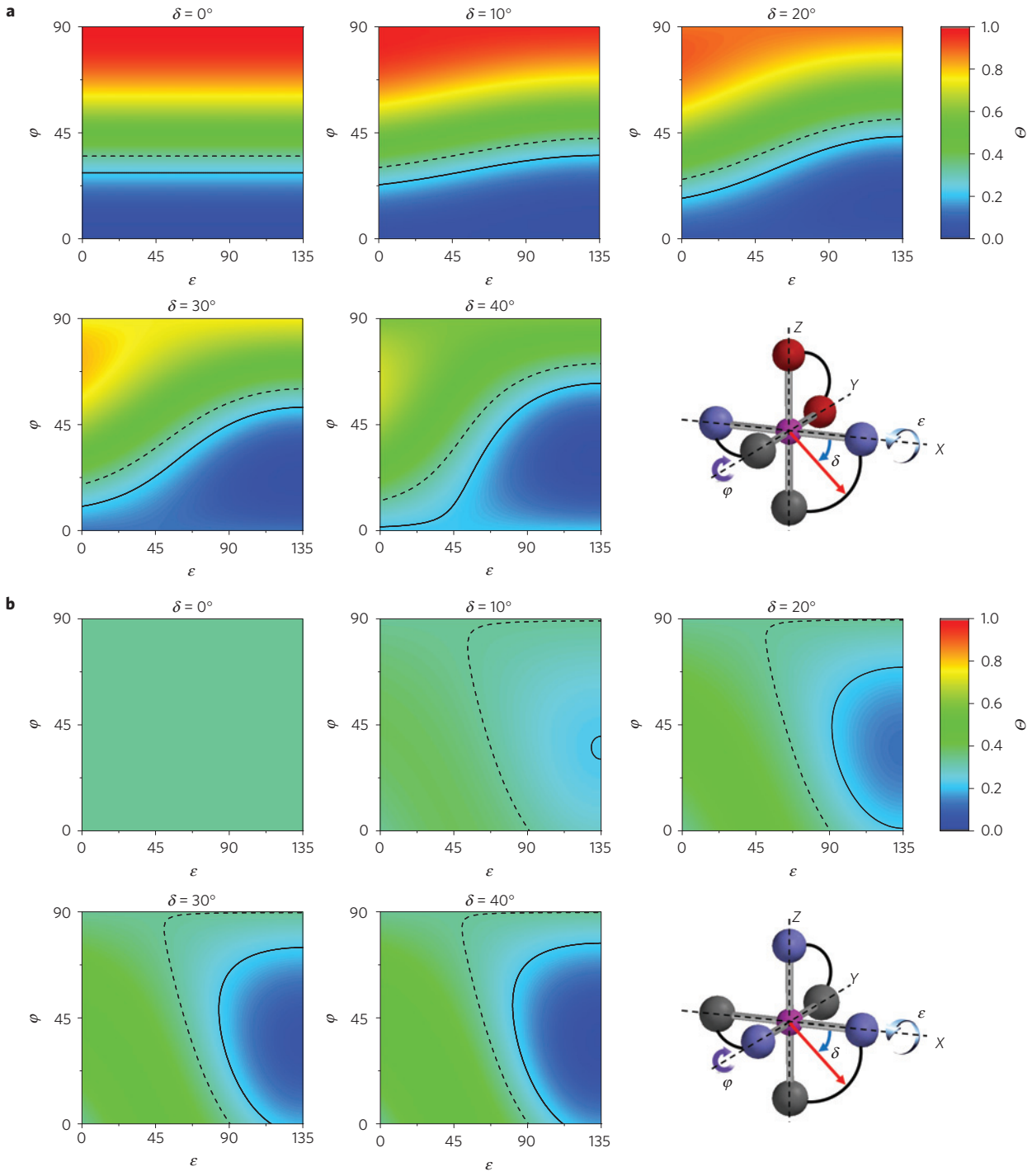

Figure 4 | Molecular orientation. a,**b**, Surface maps illustrating the dependence of the optical anisotropy parameter Θ, represented here by a colour gradient, on molecular rotation for any Ir(C^N)$_2$(O^O) molecule (**a**) or homoleptic fac-Ir(C^N)$_3$ molecule (**b**) starting from the orientation shown. The angle N–Ir–TDV is δ, where $\delta = 0°$ corresponds to a TDV oriented directly towards the nitrogen. ε is rotation about the x axis, and φ is rotation around the y axis in the direction shown in the sketch. The solid line is $\Theta = 0.22$ and the dashed line is $\Theta = 0.33$ (isotropic).

of a general (C^N)$_2$Ir(acac) and fac-Ir(C^N)$_3$ complexes affects Θ for any molecular orientation and any given TDV. The coordinate system and direction of rotation for the molecules around angles ε and φ are defined in Fig. 4, with the z axis orthogonal to the substrate. The model assumes that the TDV lies in the plane of the (C^N)Ir ligands at an angle δ between the Ir–N bond and TDV. To probe the dependence of Θ on molecular orientation for various values of δ, the metal complex is rotated in the imposed coordinate system and Θ is calculated for the molecule using equation (1) in the Methods section. The starting point for both types of complex ($\varepsilon = \varphi = 0°$) is depicted in Fig. 4. The molecules were rotated stepwise around ε and Θ was calculated from the projection of the TDV of the emissive ligand(s) onto the x, y and z directions at each step in ε and φ. Figure 4 shows one quadrant of the possible ε and φ values; full plots for ε, $\varphi = 0°$–$360°$ are presented in Supplementary Figs 15 and 16.

For (C^N)$_2$Ir(O^O) complexes, values of Θ with $\delta < 10°$ are insensitive to rotation around ε but vary with changes in φ (Fig. 4a).

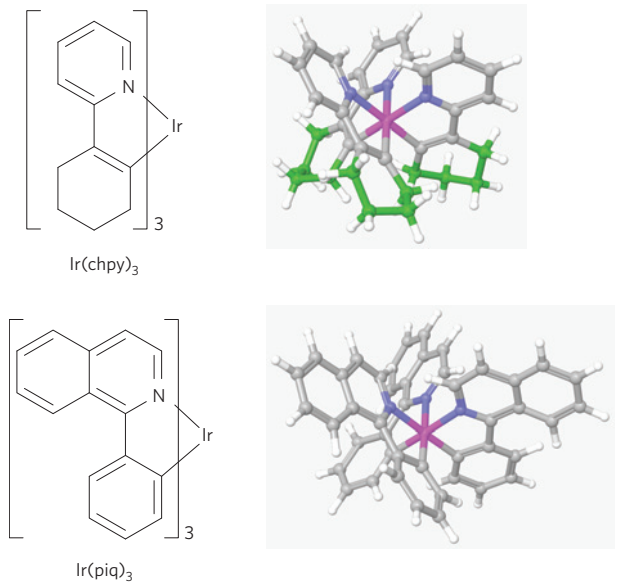

Figure 5 | Oriented homoleptic phosphors. Molecular models of two facial Ir(C^N)$_3$ complexes that align in a CBP matrix. The aliphatic carbons of the chpy ligand have been coloured green.

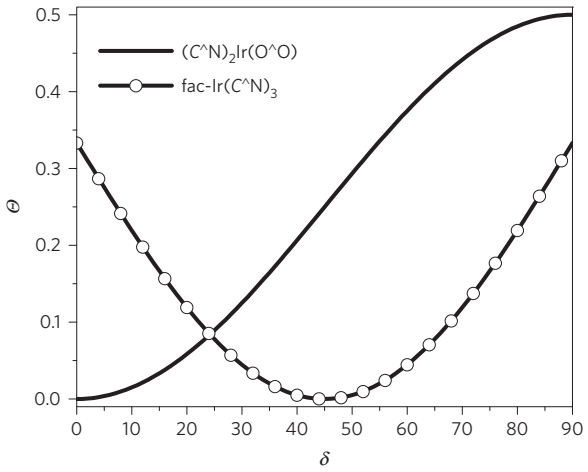

Figure 6 | Ideal molecular orientation. Plot of δ versus Θ for $(C^N)_2Ir(O^O)$ and fac-Ir$(C^N)_3$ complexes with their respective C_2 and C_3 axes oriented perpendicular to the substrate.

As the magnitude of δ increases, a dependence of Θ on rotation around ε appears. Regions of low Θ become localized near values of $\varepsilon = 135°$, which places the C_2 axis in the x–y plane, parallel to the substrate. The mechanism we propose for dopant alignment predicts that the $(bppo)_2Ir(acac)$ molecules will orient with the C_2 axis perpendicular to the substrate. We expect the bppo-based emitters to have values of δ between 20° and 40° (see above). Examination of the plots in Fig. 4a shows that if the $(bppo)_2Ir(acac)$ dopants exhibited uniform alignment with their C_2 axes orthogonal to the substrate ($\varepsilon = 45°$, 225° and $\varphi = 0°$), then Θ would be less than 0.22 for any value of $\delta \leq 40°$. The experimental values of Θ being higher than predicted is likely to come from two sources. First, random variation away from orthogonal order is expected for a population of molecules, which will shift the net orientation towards isotropic. Second, film roughness in much the same way contributes to a deviation towards an isotropic alignment. Examination of the CBP and doped CBP films by atomic force microscopy (AFM) shows that the organic films are not flat but have an r.m.s. roughness of 2.2 nm. We have evaluated random traces of the AFM image for an 8% doped CBP film (see Supplementary Information and Supplementary Fig. 14) and determined that the average angle the CBP surface takes relative to the substrate surface is 5.2° ± 0.3°. Both of these factors are expected to shift the net molecular orientation away from the ideal $\varepsilon = 45°$, 225° and $\varphi = 0°$ towards a more isotropic value. Note that when $\varepsilon < 45°$, only a small increase in φ is needed to obtain $\Theta = 0.22$ for δ values between 30° and 40°.

In contrast to $(C^N)_2Ir(O^O)$ complexes, fac-Ir$(C^N)_3$ complexes with a TDV oriented along any metal–ligand bond ($\delta = 0, 90$) will yield a Θ value of 0.33 for all molecular orientations (Fig. 4b). In this case, emission from a perfectly aligned emitter will be experimentally indistinguishable from a randomly oriented one. As the TDV deviates from the metal–ligand bond axis ($90 > \delta > 0$), regions of low Θ appear centred at angles of $\varepsilon = 135°$ and $\varphi = 35.3°$ corresponding to a molecular geometry with the C_3 axis perpendicular to the x–y plane.

There are two examples of facial homoleptic complexes that are reported to show substantial alignment in doped films (see Ir$(chpy)_3$ and Ir$(piq)_3$ in Fig. 5 and Supplementary Table 1). The Θ values for the two dopants are 0.23 and 0.22, respectively[26]. The two complexes have C^N ligands that give rise to substantial structural anisotropy in the facial tris-chelated complexes, similar to heteroleptic species, as can be seen in the structural models shown in Fig. 5 (refs 22,26). Ir$(chpy)_3$ clearly has an aromatic and an aliphatic side, whereas the difference in Ir$(piq)_3$ is more subtle. If this anisotropy orients the molecule by our proposed mechanism, we would expect the molecular C_3 axis of these molecules to orient perpendicular to the surface, and the measured Θ value would correspond to TDV angles of $\delta \approx 10°$ (Fig. 6), well within the anticipated range for these C^N ligands.

Our work demonstrates the optimal design principles for Ir-based dopants to exploit the benefits of dopant orientation in OLEDs. For $(C^N)_2Ir(O^O)$ it would be advantageous to shift the direction of the TDV towards the Ir–N bond axis, ideally to $\delta = 0°$ (Fig. 6). Note that any net orientation with $\varphi = 0°$–20° gives values of $\Theta < 0.1$ when $\delta = 0°$ (Fig. 4a). Such a broad spread of orientations is well within the range seen for the compounds reported here. The outcoupling efficiency of an OLED with $\Theta = 0.1$ would increase by roughly a factor of 1.5 as compared with the isotropic case[23]. Alternatively, if one could align the dopants more uniformly with their C_2 axis perpendicular to the substrate ($\varepsilon = 45$ or 225° and $\varphi = 0$), Θ of ≤0.1 could be achieved with δ values as high as 25° (Fig. 6). $(C^N)_2Ir(acac)$ complexes limit the operational stability of OLEDs, owing largely to the instability of the acac ligand. Heteroleptic Ir complexes, that is, $(C^N)_2Ir(C'^N')$, however, do not suffer from poor device stability. The mechanism described here, invoking structural anisotropy of the dopant to promote alignment, is equally applicable to heteroleptic complexes with aliphatic groups incorporated into either C^N or C'^N'. Figure 6 also shows that related fac-Ir$(C^N)_3$ complexes with δ values between 20° and 70°, if aligned with their C_3 axes perpendicular to the substrate, are also capable of generating highly anisotropic emission. Notably, δ values between 40° and 50° will give $\Theta < 0.01$ over a fairly broad range of ε and φ values.

Conclusion

We conclude that the presence of the acac group is responsible for the commonly measured value of $\Theta \cong 0.2$ for a large variety of $(C^N)_2Ir(acac)$ species. The acac ligand forms an aliphatic region on the surface of the otherwise aromatic Ir complex. We reason that interaction of this chemically anisotropic species at the boundary created between the vacuum and the organic surface during deposition is responsible for the observed net alignment of the TDVs of the dopants, wherein the phosphor's C_2 axis is

largely perpendicular to the plane of the substrate. This proposed mechanism for alignment is consistent with the Θ value being unaffected by aggregation of the dopant. A similar mechanism for dopant alignment can be used to explain the low Θ values reported for facial $Ir(C^{\wedge}N)_3$ complexes where the $C^{\wedge}N$ ligand itself gives rise to significant chemical anisotropy of the dopant molecule, that is, $Ir(chpy)_3$ and $Ir(piq)_3$ (ref. 26).

Future work will explore the impact of the introduction of aliphatic character to different ligands. We will also explore the impact of host materials and their physical properties on the alignment behaviour of the dopants in films.

Methods

Methods and any associated references are available in the online version of the paper.

Received 22 May 2015; accepted 21 August 2015; published online 5 October 2015

References

1. Scharber, M. C. *et al.* Design rules for donors in bulk-heterojunction solar cells—towards 10% energy-conversion efficiency. *Adv. Mater.* **18,** 789–794 (2006).
2. Jurow, M. J. *et al.* Controlling morphology and molecular packing of alkane substituted phthalocyanine blend bulk heterojunction solar cells. *J. Mater. Chem. A* **1,** 1557–1565 (2013).
3. Tsao, H. N. *et al.* The influence of morphology on high-performance polymer field-effect transistors. *Adv. Mater.* **21,** 209–212 (2009).
4. Yokoyama, D. Molecular orientation in small-molecule organic light-emitting diodes. *J. Mater. Chem.* **21,** 19187–19202 (2011).
5. Namdas, E. B., Ruseckas, A., Samuel, I. D. W., Lo, S.-C. & Burn, P. L. Photophysics of fac-tris(2-phenylpyridine) iridium(III) cored electroluminescent dendrimers in solution and films. *J. Phys. Chem. B* **108,** 1570–1577 (2004).
6. Baldo, M. A. *et al.* Highly efficient phosphorescent emission from organic electroluminescent devices. *Nature* **395,** 151–154 (1998).
7. Baldo, M. A., Lamansky, S., Burrows, P. E., Thompson, M. E. & Forrest, S. R. Very high-efficiency green organic light-emitting devices based on electrophosphorescence. *Appl. Phys. Lett.* **75,** 4–6 (1999).
8. Mladenovski, S., Neyts, K., Pavicic, D., Werner, A. & Rothe, C. Exceptionally efficient organic light emitting devices using high refractive index substrates. *Opt. Express* **17,** 7562–7570 (2009).
9. Reineke, S. *et al.* White organic light-emitting diodes with fluorescent tube efficiency. *Nature* **459,** 234–238 (2009).
10. Brütting, W., Frischeisen, J., Schmidt, T. D., Scholz, B. J. & Mayr, C. Device efficiency of organic light-emitting diodes: Progress by improved light outcoupling. *Phys. Status Solidi A* **210,** 44–65 (2013).
11. Schmidt, T. D. *et al.* Evidence for non-isotropic emitter orientation in a red phosphorescent organic light-emitting diode and its implications for determining the emitter's radiative quantum efficiency. *Appl. Phys. Lett.* **99,** 163302 (2011).
12. Forrest, S. R. The path to ubiquitous and low-cost organic electronic appliances on plastic. *Nature* **428,** 911–918 (2004).
13. Sasabe, H. & Kido, J. Development of high performance OLEDs for general lighting. *J. Mater. Chem. C* **1,** 1699–1707 (2013).
14. Sasabe, H. & Kido, J. Recent progress in phosphorescent organic light-emitting devices. *Eur. J. Org. Chem.* **2013,** 7653–7663 (2013).
15. Mayr, C., Schmidt, T. D. & Brütting, W. High-efficiency fluorescent organic light-emitting diodes enabled by triplet–triplet annihilation and horizontal emitter orientation. *Appl. Phys. Lett.* **105,** 183304 (2014).
16. Liehm, P. *et al.* Comparing the emissive dipole orientation of two similar phosphorescent green emitter molecules in highly efficient organic light-emitting diodes. *Appl. Phys. Lett.* **101,** 253304 (2012).
17. Mayr, C. & Brutting, W. Control of molecular dye orientation in organic luminescent films by the glass transition temperature of the host material. *Chem. Mater.* **27,** 2759–2762 (2015).
18. Flämmich, M. *et al.* Oriented phosphorescent emitters boost OLED efficiency. *Org. Electron.* **12,** 1663–1668 (2011).
19. Helander, M. G. *et al.* Chlorinated indium tin oxide electrodes with high work function for organic device compatibility. *Science* **332,** 944–947 (2011).
20. Lamansky, S. *et al.* Highly phosphorescent bis-cyclometalated iridium complexes: Synthesis, photophysical characterization, and use in organic light emitting diodes. *J. Am. Chem. Soc.* **123,** 4304–4312 (2001).
21. Lassiter, B. E. *et al.* Organic photovoltaics incorporating electron conducting exciton blocking layers. *Appl. Phys. Lett.* **98,** 243307 (2011).
22. Kim, K.-H. *et al.* Phosphorescent dye-based supramolecules for high-efficiency organic light-emitting diodes. *Nature Commun.* **5,** 4769 (2014).
23. Kim, K.-H., Moon, C.-K., Lee, J.-H., Kim, S.-Y. & Kim, J.-J. Highly efficient organic light-emitting diodes with phosphorescent emitters having high quantum yield and horizontal orientation of transition dipole moments. *Adv. Mater.* **26,** 3844–3847 (2014).
24. Kim, S.-Y. *et al.* Organic light-emitting diodes with 30% external quantum efficiency based on a horizontally oriented emitter. *Adv. Funct. Mater.* **23,** 3896–3900 (2013).
25. Lee, J.-H. *et al.* Finely tuned blue iridium complexes with varying horizontal emission dipole ratios and quantum yields for phosphorescent organic light-emitting diodes. *Adv. Opt. Mater.* **3,** 211–220 (2014).
26. Graf, A. *et al.* Correlating the transition dipole moment orientation of phosphorescent emitter molecules in OLEDs with basic material properties. *J. Mater. Chem. C* **2,** 10298–10304 (2014).
27. Reineke, S., Rosenow, T. C., Lüssem, B. & Leo, K. Improved high-brightness efficiency of phosphorescent organic LEDs comprising emitter molecules with small permanent dipole moments. *Adv. Mater.* **22,** 3189–3193 (2010).
28. Reineke, S., Schwartz, G., Walzer, K., Falke, M. & Leo, K. Highly phosphorescent organic mixed films: The effect of aggregation on triplet–triplet annihilation. *Appl. Phys. Lett.* **94,** 163305 (2009).
29. Kim, K.-H. *et al.* Controlling emitting dipole orientation with methyl substituents on main ligand of iridium complexes for highly efficient phosphorescent organic light-emitting diodes. *Adv. Opt. Mater.* **3,** http://dx.doi.org/10.1002/adom.201500141 (2015).
30. Moon, C.-K., Kim, K.-H., Lee, J. W. & Kim, J.-J. Influence of host molecules on emitting dipole orientation of phosphorescent iridium complexes. *Chem. Mater.* **27,** 2767–2769 (2015).
31. Ren, X. *et al.* Coumarin-based, electron-trapping iridium complexes as highly efficient and stable phosphorescent emitters for organic light-emitting diodes. *Inorg. Chem.* **49,** 1301–1303 (2010).
32. Jaguar v. Version 8.4r17 (Schrödinger LLC, 2014); www.shrodinger.com/Jaguar
33. Becke, A. D. Density-functional thermochemistry. III. The role of exact exchange. *J. Chem. Phys.* **98,** 5648–5652 (1993).
34. Hay, P. J. & Wadt, W. R. *Ab initio* effective core potentials for molecular calculations. Potentials for the transition metal atoms Sc to Hg. *J. Chem. Phys.* **82,** 270–283 (1985).
35. Stephens, P. J., Devlin, F. J., Chabalowski, C. F. & Frisch, M. J. *Ab initio* calculation of vibrational absorption and circular dichroism spectra using density functional force fields. *J. Phys. Chem.* **98,** 11623–11627 (1994).
36. Frischeisen, J., Yokoyama, D., Endo, A., Adachi, C. & Brütting, W. Increased light outcoupling efficiency in dye-doped small molecule organic light-emitting diodes with horizontally oriented emitters. *Org. Electron.* **12,** 809–817 (2011).
37. Frischeisen, J., Yokoyama, D., Adachi, C. & Brütting, W. Determination of molecular dipole orientation in doped fluorescent organic thin films by photoluminescence measurements. *Appl. Phys. Lett.* **96,** 073302 (2010).
38. Mayr, C. *et al.* Efficiency enhancement of organic light-emitting diodes incorporating a highly oriented thermally activated delayed fluorescence emitter. *Adv. Funct. Mater.* **24,** 5232–5239 (2014).
39. Weber, W. H. & Eagen, C. F. Energy transfer from an excited dye molecule to the surface plasmons of an adjacent metal. *Opt. Lett.* **4,** 236–238 (1979).
40. Kawamura, Y., Brooks, J., Brown, J. J., Sasabe, H. & Adachi, C. Intermolecular interaction and a concentration-quenching mechanism of phosphorescent Ir(III) complexes in a solid film. *Phys. Rev. Lett.* **96,** 017404 (2006).
41. Chi, Y. & Chou, P.-T. Transition-metal phosphors with cyclometalating ligands: Fundamentals and applications. *Chem. Soc. Rev.* **39,** 638–655 (2010).
42. Vanhelmont, F. W. M., Strouse, G. F., Güdel, H. U., Stückl, A. C. & Schmalle, H. W. Synthesis, crystal structure, high-resolution optical spectroscopy, and extended Hückel calculations on cyclometalated $[Re(CO)_4(ppy)]$ (ppy = 2-phenylpyridine). *J. Phys. Chem. A* **101,** 2946–2952 (1997).
43. Dalal, S. S., Walters, D. M., Lyubimov, I., de Pablo, J. J. & Ediger, M. D. Tunable molecular orientation and elevated thermal stability of vapor-deposited organic semiconductors. *Proc. Natl Acad. Sci. USA* **112,** 4227–4232 (2015).
44. Kearns, K. L. *et al.* Molecular orientation, thermal behavior and density of electron and hole transport layers and the implication on device performance for OLEDs. *Proc. SPIE* **9183,** 91830F (2014).
45. Tsai, M. H. *et al.* 3-(9-carbazolyl)carbazoles and 3,6-di(9-carbazolyl)carbazoles as effective host materials for efficient blue organic electrophosphorescence. *Adv. Mater.* **19,** 862–866 (2007).
46. Dalal, S. S., Fakhraai, Z. & Ediger, M. D. High-throughput ellipsometric characterization of vapor-deposited indomethacin glasses. *J. Phys. Chem. B* **117,** 15415–15425 (2013).

47. Brian, C. W. & Yu, L. Surface self-diffusion of organic glasses. *J. Phys. Chem. A* **117,** 13303–13309 (2013).
48. Zhu, L. *et al.* Surface self-diffusion of an organic glass. *Phys. Rev. Lett.* **106,** 256103 (2011).
49. Xing, X. *et al.* Essential differences of organic films at the molecular level via vacuum deposition and solution processes for organic light-emitting diodes. *J. Phys. Chem. C* **117,** 25405–25408 (2013).

Acknowledgements

The research described here was carried out with the support of the Universal Display Corporation, The Humboldt Foundation, Bavaria California Technology Center (BaCaTeC) and Deutsche Forschungsgemeinschaft (DFG Br 1728/16-1).
C.M. acknowledges financial support by Bayerische Forschungsstiftung.

Author contributions

M.J.J. prepared materials and samples, designed experiments and prepared the manuscript; C.M. measured molecular orientation; T.D.S. designed and prepared mathematical models; T.L. designed and prepared mathematical models; P.I.D., W.B. and M.E.T. designed and assisted with experiments and the manuscript.

Additional information

Supplementary information is available in the online version of the paper. Reprints and permissions information is available online at www.nature.com/reprints.
Correspondence and requests for materials should be addressed to M.E.T.

Competing financial interests

M.E.T. has a competing interest in the Universal Display Corporation.

Methods

Starting materials were purchased from Sigma Aldrich and used without further purification. CBP was obtained from the Universal Display Corporation. Materials were purified by gradient sublimation before use. Chloro-bridged bis-cyclometalated iridium complexes of the formula $[Ir(C^{\wedge}N)_2Cl]_2$ were synthesized according to literature procedures[50].
6H-[2]benzopyrano[4,3-b]pyridin-6-one (bppo) was synthesized according to the procedure in ref. 51.

The synthesis of Iridium(III) bis(benzopyranopyridinone)(acetylacetonate) ($(bppo)_2Ir(acac)$) involved charging a flask with the chloro-bridged bppo dimer (1.4 mmol), silver triflate (3.08 mmol), bppo ligand (3.1 mmol) and potassium carbonate (13.9 mmol) under nitrogen atmosphere. The flask was charged with dry dichloroethane and stirred at reflux overnight. The solvent was removed under vacuum and the mixture was dissolved in CH_2Cl_2. The mixture was then filtered to remove silver chloride and chromatographed in 60:40 CH_2Cl_2/ethyl acetate (v/v). The collected fraction was precipitated from CH_2Cl_2 and hexanes to yield 280 mg pure $(bppo)_2Ir(acac)$ (51%). ^{1}H NMR ($CDCl_3$): 1.86 (s, Me-acac, 6H), 5.32 (s, acac, 1H), 6.60 (dd, 2H), 7.04 (t, 2H), 7.42 (q, 2H), 7.66 (qd, 2H), 8.35 (dd, 2H). Electrospray ionization mass spectrum: $C_{29}H_{19}IrN_2O_6$ M/Z calculated 684.0872, found: 684.0851.

Iridium(III) bis(2-phenylpyridinate)(benzopyranopyridinone) ($(ppy)_2Ir(bppo)$) and iridium(III) bis(benzopyranopyridinone) (2-phenylpyridinate) ($(bppo)_2Ir(ppy)$) were synthesized by methods similar to those described in a previous report[31]. Chloro-bridged ppy dimer (0.4 mmol), silver triflate (0.88 mmol) and potassium carbonate (20 mmol) were added to a round-bottom flask under nitrogen atmosphere. The flask was charged with dry 1,2 *o*-dichlorobenzene. The reaction mixture was stirred at reflux overnight. The solvent was removed under vacuum and the residue was dissolved in CH_2Cl_2. The mixture was filtered to remove silver chloride and chromatographed in CH_2Cl_2 to yield 450 mg $(ppy)_2Ir(bppo)$ (23%) and 325 mg $(bppo)_2Ir(ppy)$ (31%). $(bppo)_2Ir(ppy)$: electrospray ionization mass spectrum of $C_{35}H_{20}IrN_3O_4$, calculated M/Z: 739.1083; found: (MH^+) 740.1144. ^{1}H NMR ($CDCL_3$): 7.95 (d, 1H), 7.79 (m, 1H), 7.76 (d, 1H), 7.68 (m, 3H), 7.59 (m, 1H), 7.57 (m, 1H), 7.50 (dd, 1H), 7.46 (dd, 1H), 7.21 (d, 1H), 7.20 (m, 1H), 7.17 (m, 3H), 7.03 (dd, 1H), 6.97 (m, 2H), 6.87 (td, 1H), 6.74 (dd, 1H).

Optical spectra. Ultraviolet–visible absorption spectra were recorded using a Hewlett-Packard 4853 diode array spectrometer. Emission spectra were measured with a QuantaMaster Photon Technology International spectrofluorometer. Excited-state lifetimes were measured by time-correlated single-photon counting (IBH Fluorocube: LED excitation source). Quantum yields were measured using a calibrated integrating sphere (Hamamatsu C9920 system xenon lamp, and model C10027 photonic multichannel analyser).

Thin-film deposition. Film deposition and characterization methods have been performed as described in our previous report[52]. The detailed method is reproduced here for completeness. Films were made in an Angstrom Engineering EvoVac 800 VTE deposition system attached to a glove box and Inficon SQS-242 deposition software was used to control deposited material thicknesses using a 6 MHz Inficon quartz monitor gold-coated crystal sensor. All film depositions in the VTE were performed at pressures $\leq 4\times10^{-4}$ Pa and with deposition rates less than 1 Å s^{-1}. Organic films were stored under a nitrogen atmosphere. Doped films on glass substrates for orientation measurements were fabricated at pressures $\leq 5\times10^{-5}$ Pa with deposition rates of about 1.5 Å s^{-1} for CBP and various dopant concentrations (v/v). Films were encapsulated with a glass cover in a nitrogen atmosphere to prevent photodegeneration on photoluminescence excitation during orientation measurements.

Orientation measurements. To determine the molecular orientation in doped films, angular-dependent photoluminescence measurements were performed. This measurement technique has been described in our previous reports and is reproduced here for completeness[38,53]. The sample was attached to a fused-silica half-cylinder prism by index-matching liquid and the emission angle was changed using a rotation stage. Spectra were recorded using a fibre optical spectrometer (SMS-500, Sphere Optics) and a polarizing filter to distinguish between *p*- and *s*-polarized light. The excitation of the samples was performed with a 375 nm cw laser diode with a fixed excitation angle of 45°. The degree of orientation of the optical TDV of the emitter molecules was determined from a numerical simulation reported previously[36].

Spin-coating. Films were spin-cast from chloroform solutions. We dissolved 1 mg of each organic compound in 1 ml chloroform. We then prepared a mixture of both solutions with 4.6 ml NPD/chloroform and 0.4 ml $Ir(MDQ)_2(acac)$/chloroform resulting in a doping concentration of 8% $Ir(MDQ)_2(acac)$:NPD. Variable angle spectroscopic ellipsometry was performed (Si-substrate used) to determine thickness and the optical constants of the films after spin-coating and drying for 1 h at room temperature. The thickness of the films was additionally checked by the fitting procedure of the angular-dependent photoluminescence emission spectra (*p*-pol for the orientation and *s*-pol for the actual thickness).

Theoretical calculations. Calculations were performed using the Jaguar 8.4 (release 17) software package on the Schrodinger Material Science Suite (v2014-2; ref. 32). Gas-phase geometry optimization was calculated using the B3LYP functional with the LACVP** basis set as implemented in Jaguar[33–35].

Electrochemistry. $(bppo)_2Ir(acac)$ shows reversible reductions at −2.06 V and −2.29 V and a reversible oxidation at 0.69 V (versus Fc^+/Fc) by cyclic voltammetry. $(bppo)_2Ir(ppy)$ shows reversible reductions at −2.12 V and −2.31 V and a reversible oxidation at 0.63 V (versus Fc^+/Fc). $(ppy)_2Ir(bppo)$ shows a fully reversible reduction at −2.19 V and a quasi-reversible reduction at −2.77 V with a reversible oxidation at 0.48 V (versus Fc^+/Fc). The reversible oxidations are assigned to a metal-centred oxidation and the observed reductions are to a ligand-centred process. The more positive oxidations and more negative reductions relative to classic phosphors are proposed to be a consequence of the introduction of the extremely electron-withdrawing coumarin ligands. These strongly π electron-deficient ligands depress the highest occupied molecular orbital energy but do not change the lowest unoccupied molecular orbital as long as the emissive state remains localized on the bppo ligand. Electrochemistry of $Ir(ppy)_2(bppo)$ has been reported previously[31].

Transition dipole moment, molecular orientation, and Θ value relationships. For a single emitting molecule containing only one possible TDV, $\mathbf{p}=(p_x,p_y,p_z)$, Θ is given by: $\Theta=p_z^2/(p_x^2+p_y^2+p_z^2)$. In molecules containing n different TDVs, or an ensemble of n differently oriented molecules, each of these TDVs must be taken into account. As an excited state is related to only one of them, each TDV must be calculated separately with respect to the contributing fraction a_i; $\sum_{i=1}^{n} a_i=1$. Thus, the resulting Θ can be calculated as in equation (1), where $\mathbf{p}_i$ denotes the ith TDV and $p_{z,i}$ the corresponding component perpendicular to the surface.

$$\theta=\frac{\sum_{i=1}^{n} a_i p_{z,i}^2}{\sum_{i=1}^{n} a_i \mathbf{p}_i^2} \quad (1)$$

To explore the relationship between the anisotropy factor Θ for different orientations of a heteroleptic Ir complex comprising one acac group and two other identical ligands $Ir(L)_2(acac)$ we have designed a coordinate system around an idealized molecule, depicted in Fig. 4a.

The biggest influence on the orientation of the molecule is achieved by the acac group. Therefore, we selected two individual angles to control the orientation of the molecule, and one to account for variations in the angle of the TDV. We define the angle N–Ir–TDV as δ, rotation around the x axis as ε and rotation around the y axis as φ.

To model the rotation of the molecule anticlockwise around the x axis we use a rotation matrix (R_x)

$$R_x=\begin{pmatrix}1 & 0 & 0\\ 0 & \cos(\epsilon) & -\sin(\epsilon)\\ 0 & \sin(\epsilon) & \cos(\epsilon)\end{pmatrix}$$

to represent the change in the position of the TDV of both ligands, using the coordinate system of the starting geometry (Fig. 4a), denoted as $\mathbf{L}_1$ (x–y plane) and $\mathbf{L}_2$ (y–z plane):

$$\mathbf{L}_1=\begin{pmatrix}-\cos(\delta)\\ -\sin(\delta)\\ 0\end{pmatrix}$$

$$\mathbf{L}_2=\begin{pmatrix}\cos(\delta)\\ 0\\ -\sin(\delta)\end{pmatrix}$$

The rotated TDV ($\mathbf{L}_1^*$ and $\mathbf{L}_2^*$) values for both ligands are obtained by multiplying the rotation matrix with the initial TDV:

$$R_x\circ\mathbf{L}_1=\mathbf{L}_1^*=\begin{pmatrix}-\cos(\delta)\\ -\sin(\delta)\cos(\epsilon)\\ -\sin(\delta)\sin(\epsilon)\end{pmatrix}$$

$$R_x\circ\mathbf{L}_2=\mathbf{L}_2^*=\begin{pmatrix}\cos(\delta)\\ \sin(\delta)\sin(\epsilon)\\ -\sin(\delta)\cos(\epsilon)\end{pmatrix}$$

However, as only the squared vectors are of interest to calculate the anisotropy factor, the total X-, Y- and Z-components are given by the sum of the individual contributions of the two vectors:

$$X = [-\cos(\delta)]^2 + [\cos(\delta)]^2$$

$$Y = [-\sin(\delta)\cos(\epsilon)]^2 + [\sin(\delta)\sin(\epsilon)]^2$$

$$Z = [-\sin(\delta)\sin(\epsilon)]^2 + [-\sin(\delta)\cos(\epsilon)]^2$$

The anisotropy factor Θ can then be calculated for arbitrary angles of δ and ε using:

$$\theta = \frac{Z}{X+Y+Z}$$

To make the analysis more extensive, one can think about a second rotation anticlockwise around the y axis (denoted with the angle φ in the following) after the x-axis rotation. It is critical to note that the order of the rotations matters. The epsilon rotation must be applied first because the axes themselves do not change, but the molecular arrangement does (after the first rotation). Analogous to the former rotation matrix, one would achieve the following values for the three individual parameters δ, ε and φ:

$$X = [-\cos(\delta)\cos(\phi) - \sin(\delta)\sin(\epsilon)\sin(\phi)]^2 + [\cos(\delta)\cos(\phi) - \sin(\delta)\cos(\epsilon)\sin(\phi)]^2$$

$$Y = [-\sin(\delta)\cos(\epsilon)]^2 + [\sin(\delta)\sin(\epsilon)]^2$$

$$Z = [\cos(\delta)\sin(\phi) - \sin(\delta)\sin(\epsilon)\cos(\phi)]^2 + [-\cos(\delta)\sin(\phi) - \sin(\delta)\cos(\epsilon)\cos(\phi)]^2$$

The same procedure can also be applied to a homoleptic tris-Ir-compound such as, for example, $Ir(ppy)_3$. Here, one has to transform/rotate three different TDVs, one for each ligand. In the case that the three nitrogens are lying in the x-, ($-y$)- and z-direction, depicted in Fig. 4b, and the rotations are again performed around the x and the y axis, the TDVs for deriving Θ change to:

$$\mathbf{L}_1' = \begin{pmatrix} -\sin(\delta)\cos(\phi) - \cos(\delta)\sin(\epsilon)\sin(\phi) \\ -\cos(\delta)\cos(\epsilon) \\ \sin(\delta)\sin(\phi) - \cos(\delta)\sin(\epsilon)\cos(\phi) \end{pmatrix}$$

$$\mathbf{L}_2' = \begin{pmatrix} \cos(\delta)\cos(\phi) - \sin(\delta)\cos(\epsilon)\sin(\phi) \\ \sin(\delta)\sin(\epsilon) \\ -\cos(\delta)\sin(\phi) - \sin(\delta)\cos(\epsilon)\cos(\phi) \end{pmatrix}$$

$$\mathbf{L}_3' = \begin{pmatrix} \sin(\delta)\sin(\epsilon)\sin(\phi) + \cos(\delta)\cos(\epsilon)\sin(\phi) \\ \sin(\delta)\cos(\epsilon) - \cos(\delta)\sin(\epsilon) \\ \sin(\delta)\sin(\epsilon)\cos(\phi) + \cos(\delta)\cos(\epsilon)\cos(\phi) \end{pmatrix}$$

References

50. Nonoyama, M. Benzo[h]quinolin-10-yl-N iridium(III) complexes. *Bull. Chem. Soc. Jpn* **47,** 767–768 (1974).
51. Zhang, W. & Pugh, G. Free radical reactions for heterocycle synthesis. Part 6: 2-bromobenzoic acids as building blocks in the construction of nitrogen heterocycles. *Tetrahedron* **59,** 3009–3018 (2003).
52. Navarro, F. F., Djurovich, P. I. & Thompson, M. E. Metal deposition for optoelectronic devices using a low vacuum vapor phase deposition (VPD) system. *Org. Electron.* **15,** 3052–3060 (2014).
53. Mayr, C., Taneda, M., Adachi, C. & Brütting, W. Different orientation of the transition dipole moments of two similar Pt(II) complexes and their potential for high efficiency organic light-emitting diodes. *Org. Electron.* **15,** 3031–3037 (2014).